

# We are IntechOpen, the world's leading publisher of Open Access books Built by scientists, for scientists

6,900

Open access books available

186,000

International authors and editors

200M

Downloads

Our authors are among the

154

Countries delivered to

TOP 1%

most cited scientists

12.2%

Contributors from top 500 universities



WEB OF SCIENCE™

Selection of our books indexed in the Book Citation Index  
in Web of Science™ Core Collection (BKCI)

Interested in publishing with us?  
Contact [book.department@intechopen.com](mailto:book.department@intechopen.com)

Numbers displayed above are based on latest data collected.  
For more information visit [www.intechopen.com](http://www.intechopen.com)



## Chapter

# Surface Science of Graphene-Based Monoliths and Their Electrical, Mechanical, and Energy Applications

*Mujtaba Ikram, Sana Arbab, Bilal Tariq, Rayha Khan, Husnain Ahmad, Abdullah Khan Durran, Muhammad Ikram, Muhammad Aamir Iqbal and Asghari Maqsood*

## Abstract

Ceramic monoliths are applied in many insulating and high resistive engineering applications, but the energy application of ceramics monoliths is still vacant due to less conductivity of monolithic ceramics (for example, in silica- and alumina-based hybrids). This book chapter is a significant contribution in the graphene industry as it explains some novel and modified fabrication techniques for ceramics-graphene hybrids. The improved physical properties may be used to set ceramics-graphene hybrids as a standard for electrical, mechanical, thermal, and energy applications. Further, silica-rGO hybrids may be used as dielectric materials for high-temperature applications due to improved dielectric properties. The fabricated nano-assembly is important for a technological point of view, which may be further applied as electrolytes, catalysts, and conductive, electrochemically active, and dielectric materials for the high-temperature applications. In the end, this chapter discussed porous carbon as a massive source of electrochemical energy for supercapacitors and lithium-ion batteries. Carbon materials which are future of energy storage devices because of their ability to store energy in great capacity, so sustainability through smart materials got a huge potential, so hereby keeping in view all the technological aspects, this chapters sums up important contribution of graphene and porous carbon for applied applications.

**Keywords:** graphene, ceramics, superior energy storage, chemical activation, supercapacitors, lithium-ion batteries

## 1. Introduction

Decades ago, scientists believed that carbon comes in two basic forms, that is, graphite and diamond, but in the last three decades, scientists have discovered new forms of carbon known as advanced carbon materials including fullerene, carbon nanotubes (CNTS), and graphene, respectively [1–6]. In recent years, graphene

is considered as an outstanding candidate for enhancing the structural, electrical, mechanical, and thermal properties of materials (for example, metals, ceramics, and polymers) [7, 8]. In hybrid nanostructures, the physical property enhancement may be possible due to excellent physical properties of the graphene. Excellent physical properties included higher thermal conductivity ( $5000 \text{ Wm}^{-1} \text{ K}^{-1}$ ), electrical conductivity ( $10^6 \text{ S m}^{-1}$ ), and Young's modulus (1 TPa), which are a driving force for enhancement in the physical properties of hybrids. Among the various types of graphene materials, graphite oxide-derived graphene plays an important role in increasing the physical properties of hybrids because of its surface functionalization and its ability of large-scale production at any level. Even a tiny amount of graphene in hybrids (either polymers or ceramics or metals) may alter its physical properties to a great extent. In case of graphene, the compatible structural properties and how it makes bond with various types of nanostructures are reasons for improved properties in the end product (hybrids or composites). For example, reduced graphite oxide (rGO)-polystyrene composites with a low threshold content of 0.1 (volume %) rGO have shown greatly improved electrical conductivity (approx.  $0.1 \text{ S m}^{-1}$ ); this has been possible due to good dispersion of rGO in the polymer composite matrix. Similarly, in inorganic hybrids, rGO has been used for the deposition of  $\text{Co}_3\text{O}_4$  particles for increased catalytic effects, which may have been used for the decomposition of ammonium perchlorate because of the complex properties of GO and  $\text{Co}_3\text{O}_4$ . In another research, rGO was used to improve the mechanical properties of the bulk silicon nitride (i.e. toughness is enhanced by up to 235%), which may be used for high-performance mechanical and structural applications [8, 9]. In short, graphene being the toughest, strongest, lightweight material may act as a wonder material for future scientific revolution in every aspect of life. Even if it is combined with polymers, metals, and ceramics, it may play a significant role in improving physical properties due to its versatile surface, morphology, chemistry, and physical properties. In this chapter, we will discuss graphene combination with various ceramics and how it has been used to improve their physical properties, and porous carbon for energy storage, respectively. This book chapter will be a significant contribution to advance studies on physical properties and technological applications.

## 2. Highly conductive graphene-alumina-based hybrid monoliths for electrical, thermal, and mechanical applications

Low strength and brittle attributes are the main properties of ceramics. The most widely used structural ceramic is alumina, due to its good thermal conductivity and the shape stability [7]. Alumina has a wide range of applications, some of the fields include dental implants, high speed cutting tools, chemical insulators, electrical insulators, and wear resistant coatings. Scientists have observed that mechanical properties of alumina may be improved using carbon nanotubes, for example, fracture toughness (by 94%), flexural strength (6.4%), and hardness (by 13%), respectively. On the addition of graphene platelets, about 40% enhancement in the fracture toughness of the ball milled alumina/zircon/graphene have been noticed. In another research study, the alumina-rGO core shell nanocomposites were fabricated using the method known as the sol-gel method, and it was found through this study that the BET surface area of the rGO is essential to enhance the surface charge properties of the hybrids. In another study, alumina graphene composite films were reported with a low optical gap of about 1.53 eV. Alumina-rGO nano-composites obtained via deposition during the process showed a unique morphology of aluminum nanoparticles with low prosperity and BET surface area of  $242.4 \text{ m}^2 \text{ g}^{-1}$ .

Moreover, scientists have found that in a microwave preparation of alumina-rGO composites, the grain size of the alumina matrix was reduced from 475 to 180 nm, which was obtained from the conventional sintering process, leading to an increase in the Young's modulus from 148 to 180 GPa. Scientists have found that using solvothermal-hot press processing route, highly conductive alumina-rGO hybrids may be obtained, which consist of Al<sub>2</sub>O<sub>3</sub> nanorods and rGO, respectively [7, 8, 10]. The same solvothermal method was used to form hybrids from cross-linked Al<sub>2</sub>O<sub>3</sub> nanorods and reduced graphite oxide (rGO) platelets. Then after hot pressing, the hybrid monoliths were obtained, which were utilized for the systematical study of improved physical properties of hybrids. Using the same method, it is noticed that with the 3 h-calcinated hybrid, the Al<sub>2</sub>O<sub>3</sub>-rGO monoliths show enhanced electrical conductivity (changes from  $5.1 \times 10^{-10}$  to  $6.7 \times 10^1$  S m<sup>-1</sup>), mechanical tensile strength (90% increase), thermal conductivity (80% increase), and a much higher dielectric constant (12 times) than the bare Al<sub>2</sub>O<sub>3</sub>. The highest values of electrical conductivity ( $8.2 \times 10^1$  S m<sup>-1</sup>), thermal conductivity ( $2.53$  Wm<sup>-1</sup> K<sup>-1</sup>), dielectric constant ( $10^4$ ), and Young's modulus (3.7 GPa) are determined for the alumina-rGO hybrid which is calcinated for about 1 h. It was noticed that the functional groups that contain oxygen on GO were useful for the adsorption of aluminum isopropoxide, leading to the dispersion of rGO and the Al<sub>2</sub>O<sub>3</sub>, which were obtained during the solvothermal process by the hydrolysis of the aluminum isopropoxide [7]. The improvement in the mechanical properties was caused due to the elongated Al<sub>2</sub>O<sub>3</sub> nanorods, which was indicated by the study of aspect ratio of the nanorods. Graphene platelets, functional groups present, and their surface properties are driving forces for enhancement in the physical properties of alumina-rGO hybrids.

## **2.1 Preparations of highly conductive graphene-alumina-based hybrid monoliths**

In the past, alumina rGO hybrids have been prepared using sol gel, molecular level mixing, and powder coating methods, but scientists have tried some conventional preparation methods followed by high temperature treatments [7, 11]. Such methods have shown great enhancement in physical properties of hybrids. Here, we discuss one of such advanced methods, that is, the preparation of Al<sub>2</sub>O<sub>3</sub>-rGO hybrids using solvothermal-hot press processing route. Al<sub>2</sub>O<sub>3</sub>-rGO was prepared by the mixing of GO and with cyclohexane and the aluminum isopropoxide (C<sub>9</sub>H<sub>21</sub>AlO<sub>3</sub>), which was followed by the solvothermal process. The procedure involves 0.1 g of GO being first dispersed in 35 mL of cyclohexane, then 3.5 mL of aluminum isopropoxide (C<sub>9</sub>H<sub>21</sub>AlO<sub>3</sub>) being added dropwise. The mixture is then stirred continuously at room temperature at the rate of 1000 rpm for several days until the GO powder is dispersed homogeneously but the color of the suspension changes with time. Then the products are separated by centrifugation, and the products were then washed several times with cyclohexane. The solid sample obtained are denoted as Al[O]<sub>x</sub>/GO. Then it was sent for the hydrothermal treatment. For this, it was dispersed in 50 mL cyclohexane and then transferred to the 100 mL Teflon-lined stainless steel autoclave, after which the reaction was carried out for about 6 h at about 453 K, and the resultant sample was again centrifuged and dried at about 303 K, which is denoted as Al[O]<sub>x</sub>/rGO. It was then calcined at 723 K for about 1–3 h to form Al<sub>2</sub>O<sub>3</sub>/rGO hybrids. The condition of calcination is limited supply of air. The calcination process was controlled by using the quartz tubular furnace with open ends that will allow the calcination to occur in the limited supply of air; also, the furnace was heated to the desired temperature of about 723 K for the calcination times for 1–3 h. In the initial stage, the temperature was increased by using heating rate of about 15°C min<sup>-1</sup>. As a result, the free standing

Al<sub>2</sub>O<sub>3</sub> nanorods were formed as a result of calcination treatment and also the GO was reduced to rGO. The physical properties were studied by obtaining the Al<sub>2</sub>O<sub>3</sub>/rGO hybrid powder samples consisting of 16.707, 12.830, and 7.705 wt% using the same solvothermal process. The same process was then used for the preparation of the pure Al<sub>2</sub>O<sub>3</sub> without the addition of GO. The calcination temperature was altered and was set at different temperatures for the processing time of about 1 h. For the analysis of crystallinity, it was set as 500, 600, 650, 700, 750, and 800 K and for the analysis of the effect of calcination temperature and time on the nanorods structure, the calcination time was set as 1, 2, 3, 4, and 5 h for the temperature of 723, 823, and 923 K. Hot pressing of powder samples was carried out in a vacuum furnace. The furnace was fitted with a hydraulic press which compresses the samples in a graphite pressing die. The heating temperature was made such that to increase from the room temperature at the heating rate of 10°C min<sup>-1</sup> up to 900°C, which was then maintained constant for about 60 min. When the hybrids reached the set temperature, the pressure of about 25–30 MPa was then applied to the hybrids.

## 2.2 Improved physical properties of the highly conductive graphene-alumina based hybrid monoliths

In the case of hybrids, higher the rGO, higher will be the enhancement in the physical properties such as electrical, thermal, dielectric, and mechanical properties. In the hybrids, the surface area has been increased, and as a result, greater will be the interfacial interaction of the rGO [7, 12]. The higher rGO platelets will improve the physical properties because it provides a large surface area for interfacial interactions at nano-level. Due to higher surface area of graphene, BET surface area has been improved in the hybrids as represented in the **Table 1**, in comparison with various fabrication methods [7]. Scientists believe that the higher mechanical strength is caused due to the elongated dimensions of nanorods in alumina-rGO hybrids. From the literature, it is found that 90% increase in tensile strength and 75% increase in compressive strength occur when the content of rGO is increased up to 7.707% in the hybrid. The addition of rGO affects the dielectric constant, and it increases by four orders of magnitude through a second percolation threshold [7, 8].

Further, the hot press processing sustains the quality of rGO in the hybrids. An increase in calcination temperature resulted in enhanced crystallinity in the Al<sub>2</sub>O<sub>3</sub> nanorods and rGO hybrids as also shown in XRD of hybrid (**Figure 1a**). From the surface science point of view, this may cause enhancement in the diameters and lengths of the nanorods in the hybrid as shown in the **Figure 1b**. TEM images showing variations in diameters of nano-rod structures with various calcination temperatures are presented in **Figure 1c–h**. As a result, after calcination and hot-press processing, Al<sub>2</sub>O<sub>3</sub>-rGO monoliths were obtained with enhanced physical properties. Researchers have found that with very little rGO in the alumina hybrid, higher electrical conductivity ( $8.2 \times 10^1 \text{ S m}^{-1}$ ), higher dielectric constant by four orders of magnitude, and improved thermal conductivity ( $1.4 \text{ Wm}^{-1} \text{ K}^{-1}$ ) have been achieved [7]. Hot pressing at 900°C ensured the complete reduction of GO and the higher crystallinity of Al<sub>2</sub>O<sub>3</sub>, resulting in enhanced physical properties. The elongated and fine Al<sub>2</sub>O<sub>3</sub> nanorod morphology, atomic-level layered structure, and excess surface free electrons of rGO resulted in the best reported BET surface area ( $408 \text{ m}^2 \text{ g}^{-1}$  in the 2 h-calcinated alumina-rGO), best thermal conductivity ( $2.53 \text{ Wm}^{-1} \text{ K}^{-1}$  in the 1 h-calcinated alumina-rGO), and relatively small density ( $0.92 \text{ g cm}^3$  in the 1 h-calcinated alumina-rGO) and high strength (3.7 GPa in the 1 h-calcinated alumina-rGO), respectively [7].

Sample type	BET surface area (m <sup>2</sup> g <sup>-1</sup> )				Bulk density (g/cm <sup>3</sup> )			
	$\gamma$ -Al <sub>2</sub> O <sub>3</sub> (1 h calcination time)	$\gamma$ -Al <sub>2</sub> O <sub>3</sub> -rGO (3 h calcination time)	$\gamma$ -Al <sub>2</sub> O <sub>3</sub> -rGO (2 h calcination time)	$\gamma$ -Al <sub>2</sub> O <sub>3</sub> -rGO (1 h calcination time)	$\gamma$ -Al <sub>2</sub> O <sub>3</sub> (1 h calcination time)	$\gamma$ -Al <sub>2</sub> O <sub>3</sub> -rGO (3 h calcination time)	$\gamma$ -Al <sub>2</sub> O <sub>3</sub> -rGO (2 h calcination time)	$\gamma$ -Al <sub>2</sub> O <sub>3</sub> -rGO (1 h calcination time)
Solvothermal-hot press processing method	280	361	408	379	2.75	1.61	1.37	0.92
Meso-porous Al <sub>2</sub> O <sub>3</sub> -rGO	Al <sub>2</sub> O <sub>3</sub>			Al <sub>2</sub> O <sub>3</sub> -rGO		Al <sub>2</sub> O <sub>3</sub>		Al <sub>2</sub> O <sub>3</sub> -rGO
	243			327		2.40		1.65
Core-shell flakes Al <sub>2</sub> O <sub>3</sub> -rGO	Al <sub>2</sub> O <sub>3</sub>			Al <sub>2</sub> O <sub>3</sub> -rGO		Al <sub>2</sub> O <sub>3</sub>		Al <sub>2</sub> O <sub>3</sub> -rGO
	286.62			119.71		2.816		0.003
In situ deposition Al <sub>2</sub> O <sub>3</sub> -rGO	Al <sub>2</sub> O <sub>3</sub>			Al <sub>2</sub> O <sub>3</sub> -rGO		Al <sub>2</sub> O <sub>3</sub>		Al <sub>2</sub> O <sub>3</sub> -rGO
	N/A			242.4		N/A		N/A

**Table 1.** BET surface area and density comparison for  $\gamma$ -Al<sub>2</sub>O<sub>3</sub>-rGO (1, 2 and 3 h calcination time) and pure  $\gamma$ -Al<sub>2</sub>O<sub>3</sub> (1 h calcination time), compared with various fabrication methods [7].

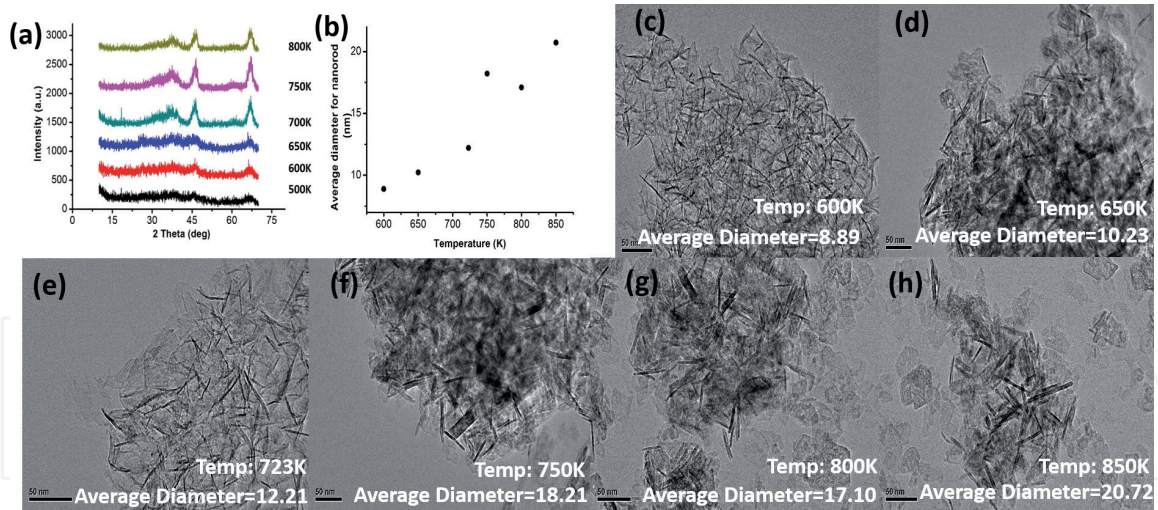


**Figure 1.** (a) XRD of  $\gamma$ - $\text{Al}_2\text{O}_3$ -rGO hybrids taken from 500 to 800 K, (b) average diameter of nano rods (nm) as function of calcination temperature (K), and (c-h) TEM images showing variations in diameters of nano rod structures with various calcination temperatures. Units for diameters are in (nm).

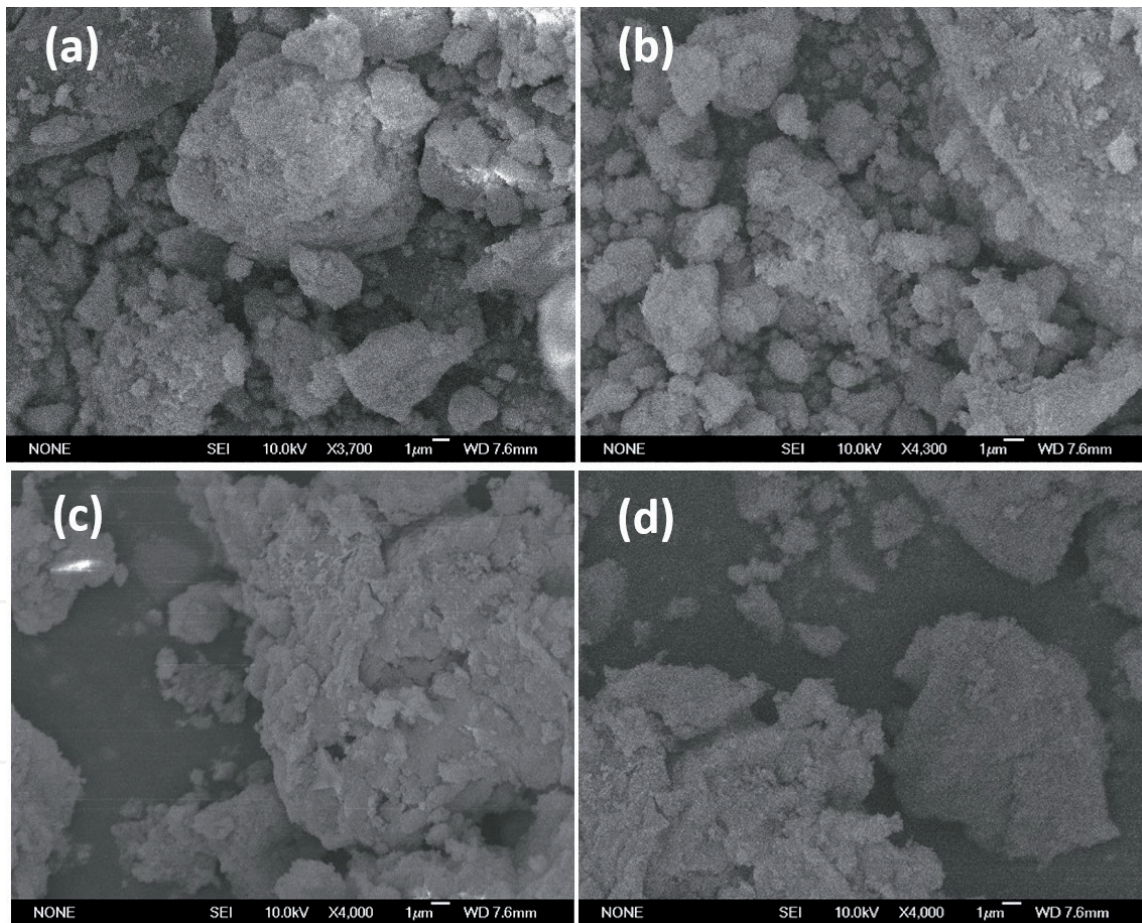


**Figure 2.** SEM images of hot pressed samples: (a)  $\gamma$ - $\text{Al}_2\text{O}_3$ -rGO (1 h calcination time), (b)  $\gamma$ - $\text{Al}_2\text{O}_3$ -rGO (2 h calcination time), (c)  $\gamma$ - $\text{Al}_2\text{O}_3$ -rGO (3 h calcination time), and (d) pure  $\gamma$ - $\text{Al}_2\text{O}_3$  (1 h calcination time).

Hot press processing may have an impact on the physical properties of hybrids; SEM images of hot pressed samples have shown particle-like morphology, as represented in **Figure 2**.

Moreover, well-aligned, elongated, and fine nanorod morphology of alumina is the reason for improvement in the mechanical strength [7, 13, 14]. Aspect ratio

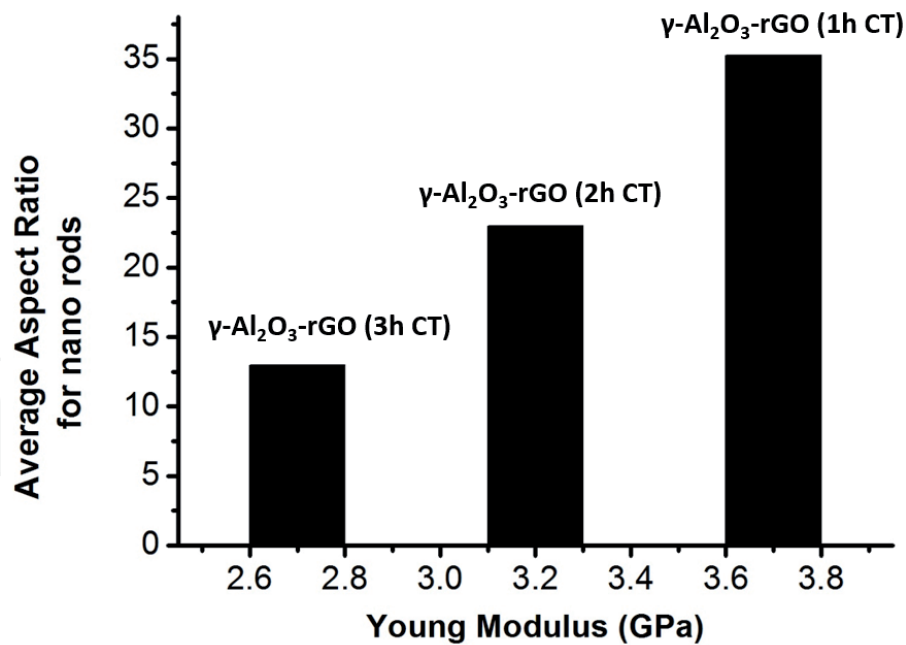


**Figure 3.** Young's modulus as a function of average aspect ratio of nano-rods in hot pressed samples  $\gamma$ - $\text{Al}_2\text{O}_3$ -rGO hybrids with 1, 2, and 3 h calcination time.

studies have confirmed that alumina-rGO hybrids (1 h calcinated) have more strength compared to hybrids that are calcined at more time (2 and 3 h), as shown in **Figure 3**.

Thus, nano-hybrids of alumina monoliths and rGO can be further applied as electrolytes, catalysts, and electrochemically active materials because of nanometer dimensions and improved physical properties [7, 15].

### 3. Highly conductive graphene-silica-based hybrid monoliths for dielectric applications

Improved physical properties may be achieved for  $\text{SiO}_2$ -rGO monoliths using calcination followed by hot press processing. If adsorption of ethyl silicate ( $\text{C}_{10}\text{H}_{20}\text{O}_4\text{Si}$ ) is required as if the group on graphene oxide contains oxygen, then it is beneficial for adsorption because it helps in uniform dispersion of rGO within the  $\text{SiO}_2$  matrix, which can be obtained during the hydrothermal reaction by hydrolysis of ethyl silicate [8, 16]. If  $\text{SiO}_2$  spheres in hybrids become more crystalline, then good physical properties in the hybrid can be obtained. Crystallinity in the  $\text{SiO}_2$  spheres can be enhanced by increasing calcination temperature and further hot press processing at  $750^\circ\text{C}$ . Graphene is a material having good physical properties. As experimentally proved by scientists worldwide, the thermal, electrical, and mechanical properties of polymers, metals, and ceramics may be improved using graphene. Graphite oxide-derived graphene has tunable surface functionalization and the potential for large scale production, so it can be used to enhance the physical properties of hybrids. For the decomposition of ammonium perchlorate,  $\text{Co}_3\text{O}_4$  can be used as a catalyst [8, 17]. To increase the catalytic effect of  $\text{Co}_3\text{O}_4$ , rGO can be used. Basically, rGO helps in uniform deposition of  $\text{Co}_3\text{O}_4$  in inorganic hybrids. Silica has good functionalized ability and is very stable, so it can be used as an additive in numerous applications. In biomedical, polymer, and ceramics engineering, silica is used for various purposes. rGO can be

used to enhance the physical properties of silica. Epoxy- $\text{SiO}_2$ -rGO hybrids have enhanced thermal conductivity ( $0.452 \text{ W m}^{-1} \text{ K}^{-1}$ ), storage modulus (3.56), and dielectric constant (77.23). In another study, rGO has been used to improve the gas sensing performance, which was obtained by an electrostatic self-assembly approach. If dispersion, corrosion resistance, and barrier properties of hybrids are required to be enhanced, then the presence of rGO is essential, and this was found when nanocomposites of silica-graphene oxide were fabricated using in situ gel method.  $\text{SiO}_2$ -graphene hybrids are better gas sensors as compared to rGO-based sensors [18, 19]. Toward 50 ppm  $\text{NH}_3$  for 850 s, the gas sensing response of rGO-based sensors is 1.5% and that of  $\text{SiO}_2$ -graphene-based sensors is 31.5%, respectively. It has been shown that  $\text{SiO}_2$ -rGO composites having enhanced BET surface area ( $676 \text{ m}^2 \text{ g}^{-1}$ ) can be obtained by one-step hydrothermal method. On addition of ultrathin graphene,  $\text{SiO}_2$ -polyvinylidene fluoride having high dielectric constant (72.94) and low dielectric loss (0.059) is obtained. Composites of epoxy-silica-graphene oxide have enhanced tensile strength, which leads to an increase in fracture toughness and Young's modulus [8]. The physical properties of  $\text{SiO}_2$ -rGO such as dielectric, electrical, mechanical, and thermal properties need to be improved further. So, in this chapter, we are discussing various physical properties of silica-rGO hybrids for dielectric applications.

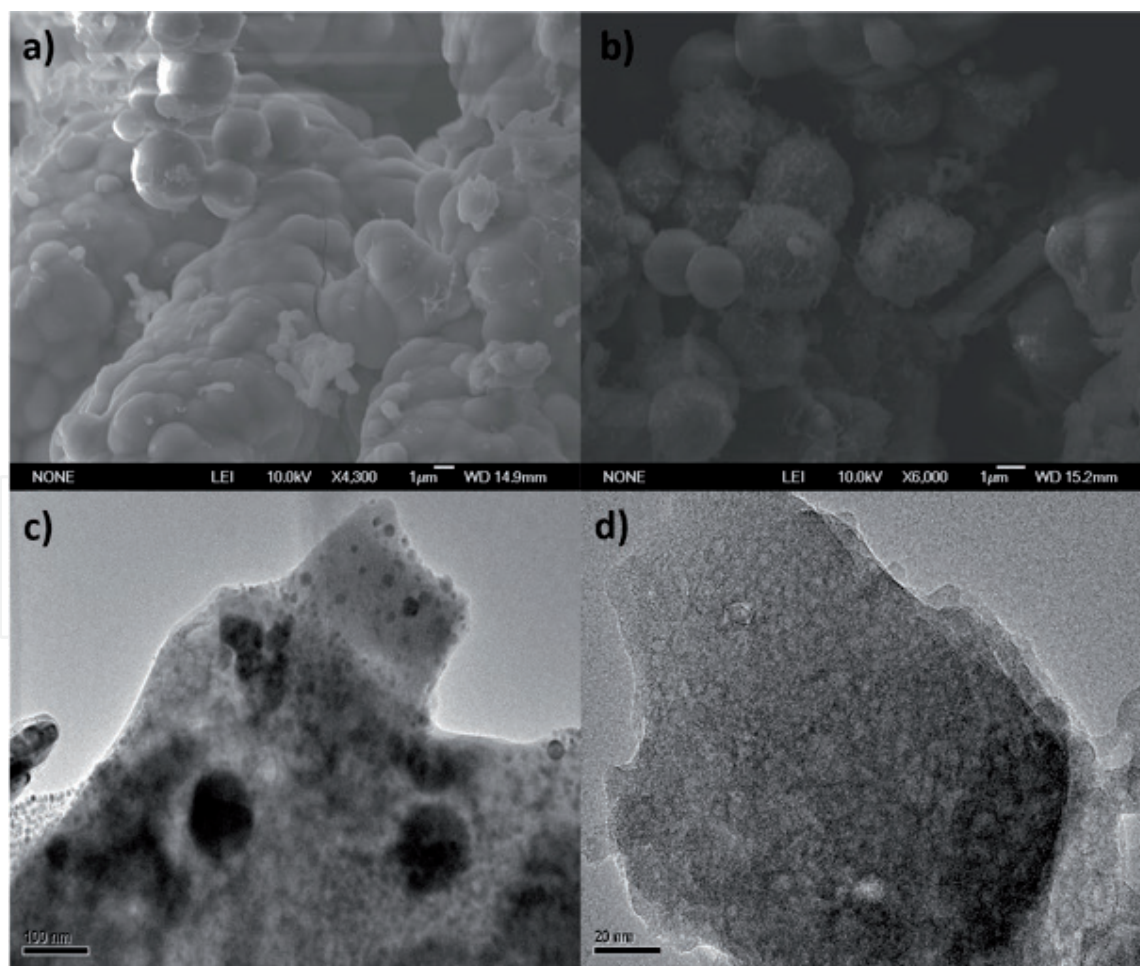


**Figure 4.**

SEM images of (a)  $\text{SiO}_2$ -rGO-6.75% (sample b) and (b)  $\text{SiO}_2$ -rGO-10.80% (sample c) fabricated at calcination temperature of 800 K for 1-h. (c) TEM images of the same  $\text{SiO}_2$ -rGO-10.80% (sample c) at lower magnification and (d) at higher magnifications.

### 3.1 Preparation of highly conductive graphene-silica based hybrid monoliths for dielectric applications

In brief preparation using solvothermal-hot press processing route [8], GO is mixed with cyclohexane and ethylsilicate ( $C_{10}H_{20}O_4Si$ ), followed by hydrothermal reaction to form  $SiO_2$ -rGO hybrids. For the preparation, 0.1 g of GO is dispersed in 50 mL cyclohexane, followed by addition of 5 mL of ethylsilicate dropwise. Then GO powder is homogeneously dispersed by stirring the mixture at the speed of 1500 rpm for several days at room temperature. The products are then separated by using centrifugation. The products are then washed with cyclohexane for several times. The obtained solid samples are represented as  $Si(O)_x$ /GO. From suspension of 0.1, 0.2 and 0.3 g GO,  $Si(O)_x$ /GO powders were obtained, respectively. The solid samples obtained are then dispersed in 75 mL cyclohexane, and then for hydrothermal reaction, the mixture is transferred to a 100 mL Teflon-lined stainless-steel autoclave. The reaction is then carried out at 420 K for 4 h, and the sample obtained is then centrifuged and dried at 303 K. The sample obtained is denoted as  $Si(O)_x$ -rGO. Then calcination of  $Si(O)_x$ -rGO is carried out at 800 K for 1 h. To study the physical properties, using the same method, hybrids of  $SiO_2$ -rGO consisting of 1.55, 6.75, and 10.82 wt% rGO are obtained. 1.55, 6.75, and 10.82% rGO is referred to as sample-a, sample-b, and sample-c, respectively. Without adding GO by using the same procedure, pure  $SiO_2$  (referred to as sample-d) is obtained. The calcination temperature is then set as 500, 600, 700, and 800 K for a processing time of 1 h to study the effect of calcination temperature on crystallinity.

### 3.2 Surface and physical properties of highly conductive graphene-silica-based hybrid monoliths for dielectric applications

Researchers have developed a hydrothermal-hot press processing technique, a simple and efficient method that can improve the thermal, electrical, dielectric, and mechanical properties of the hybrid [8, 20]. By a hydrothermal reaction, GO is dispersed in cyclohexane and ethylsilicate to produce hybrids composed of rGO and silica monoliths [20, 21]. The SEM morphology of hybrids has shown sphere-particle-like morphology with thin layers of rGO, which act as a support for elongated matrix, as shown in **Figure 4**.

SEM images of  $SiO_2$ -rGO-1.55% (sample a) at various temperatures are shown in **Figure 5**. At all temperatures, hybrids have shown sphere-like morphology, but sphere size changes at various temperatures [9, 22].

The solvothermal-hot press processing method shows the best reported electrical conductivity ( $0.143 \text{ S m}^{-1}$ ), thermal conductivity ( $1.612 \text{ W m}^{-1} \text{ K}^{-1}$ ), and higher dielectric constants for  $SiO_2$ -rGO monoliths. Thus, due to enhanced physical properties of the nano hybrids, it can be applied as electrolytes, catalysts, conductive and electrochemically active materials, and dielectrics for high-temperature applications [8, 12, 23].

**Table 2** have shown BET surface area and mesoporous volume % analysis for the hybrids. From the table, it is confirmed that BET surface area has been increased with more rGO in the hybrids, while mesoporous volume % increased with more silica [8, 24].

The dielectric properties of the  $SiO_2$ -rGO hybrids and bare  $SiO_2$  were measured using an LCR meter as shown in **Figure 6**. The dielectric properties of the hybrids were measured at a frequency of 1 kHz. For  $SiO_2$ , its dielectric constant is found

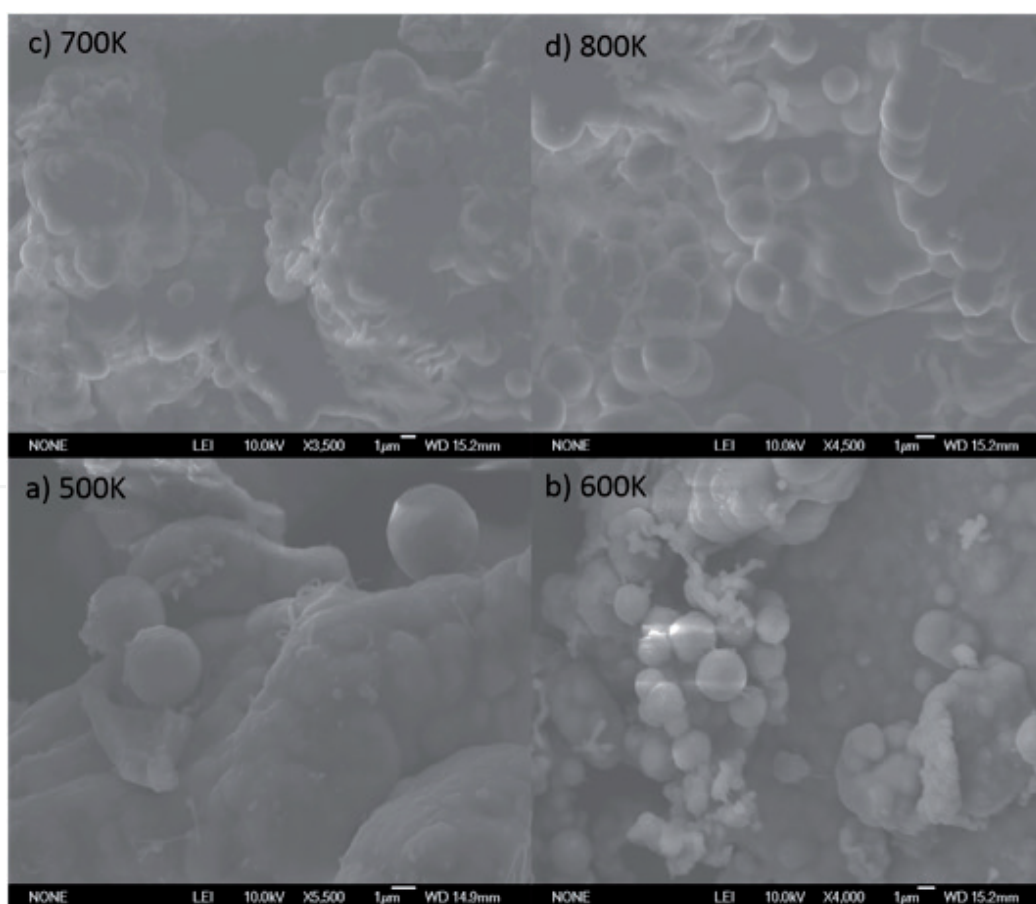


**Figure 5.** SEM images of  $\text{SiO}_2\text{-rGO-1.55\%}$  (sample a) at a calcination temperature of (a) 500 K, (b) 600 K, (c) 700 K, and (d) 800 K, respectively.

Sample type	BET surface area ( $\text{m}^2 \text{g}^{-1}$ )	Total volume ( $\text{cm}^3 \text{g}^{-1}$ )	Mesoporous volume ( $\text{cm}^3 \text{g}^{-1}$ )	Microporous volume ( $\text{cm}^3 \text{g}^{-1}$ )	Mesoporous volume (%)
Pure $\text{SiO}_2$	333.07	0.3821	0.3459	0.0362	90.52
$\text{SiO}_2\text{-rGO-1.55}$	611.21	0.4580	0.3694	0.0886	80.65
$\text{SiO}_2\text{-rGO-6.75}$	677.53	0.5521	0.3571	0.1950	64.68
$\text{SiO}_2\text{-rGO-10.8\%}$	712.01	0.6812	0.3891	0.2921	57.11

**Table 2.** BET surface area, mesoporous volume % of  $\text{SiO}_2$  (sample d),  $\text{SiO}_2\text{-rGO-1.55\%}$  (sample a),  $\text{SiO}_2\text{-rGO-6.75\%}$  (sample b), and  $\text{SiO}_2\text{-rGO-10.82\%}$  (sample c).

to be around 3.79, which is closer to that of pure silica. For sample a, the dielectric constant significantly increased by a value of 497, which indicates the presence and proximity of a first percolation threshold.

The enhanced dielectric constant (up to order of 105 and 107) was determined for samples b and c, which is much higher compared to that for sample d. Formation of conductive pathways is one of the main reasons for an increase in the overall dielectric constants. In sample c, significant leakage current leads to higher dielectric loss (300). By further increasing the rGO, the dielectric constant increased by seven orders of magnitude, indicating the presence of a second percolation

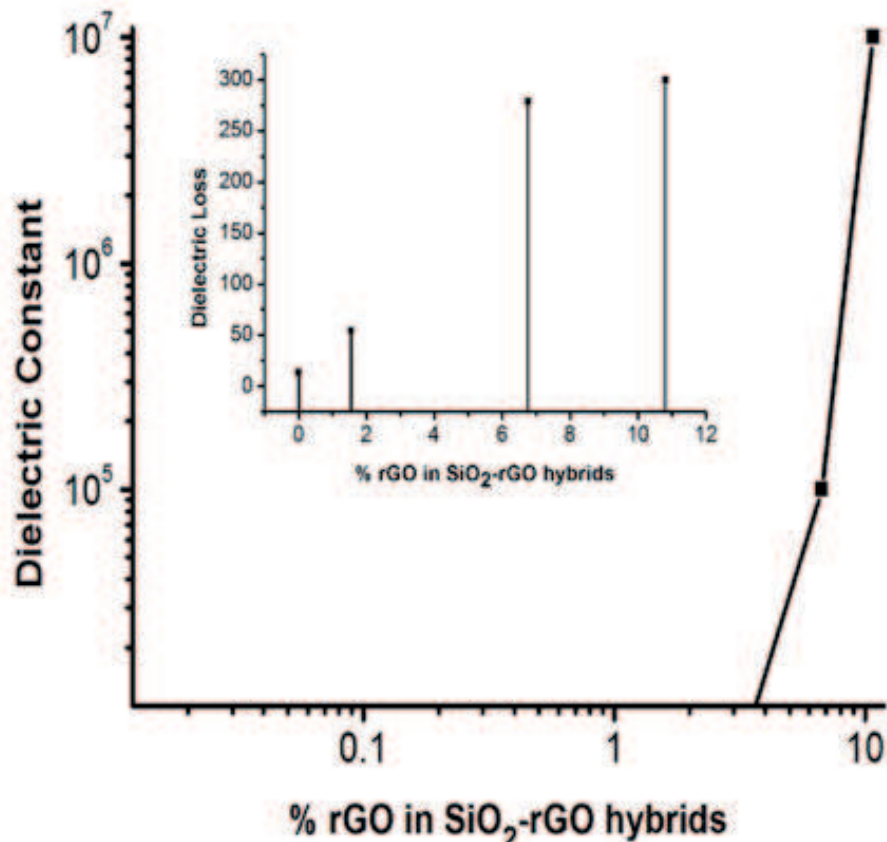


**Figure 6.** Dielectric constant as a function of % rGO in the hybrid; inset is dielectric loss as a function of % rGO in the hybrid.

threshold, which is achieved through the higher value of dielectric constant. Similarly, the dielectric loss indicates very similar behavior in the real part of the dielectric constant as shown in the inset of **Figure 6**. Scientists have experimentally proved that a small amount of rGO in hybrids can enhance dielectric properties to a great extent. The existence of a double percolation threshold in SiO<sub>2</sub> and the rGO hybrids can be significant for applied applications because it can be used to enhance the dielectric permittivity (up to 107) with the addition of a small percentage of rGO in the hybrids. Silica-rGO hybrids may be used as dielectric materials for high-temperature applications due to better dielectric properties [7, 8, 23, 25].

#### 4. Porous carbon for superior energy storage

A process called one-step carbonization-activation which is used to transform frozen tofu, mainly a source of carbon (C) and nitrogen (N), into a co-doped porous carbon having N (0.6–6.7 wt%) and O (3.6–9.5 wt %) and bearing a specific area of about  $3134 \text{ m}^2 \text{ g}^{-1}$ . Mesopores and micropores constitute a high volume of this hierarchy carbon, i.e.  $1.11 \text{ cm}^3 \text{ g}^{-1}$  consists of mesopores and  $0.71 \text{ cm}^3 \text{ g}^{-1}$  of micropores with a regular pore size appropriation somewhere in the range of 0.8–4 nm [9, 26]. When used as electrodes in supercapacitors, this porous carbon shows a specific capacitance of  $243 \text{ F g}^{-1}$  with sulfuric acid used as electrolyte and retains 93% of its initial capacitance after 10,000 cycles. In 1-butyl-3-methylimidazolium tetrafluoroborate (BMIMBF<sub>4</sub>), a specific resistance of  $170 \text{ F g}^{-1}$  and a reliable rate capability can be observed using above prepared carbon which also provides an energy density of  $72 \text{ W h kg}^{-1}$  (calculated at an average power density

of  $889 \text{ W kg}^{-1}$ ). A total of 25 light emitting diodes (LEDs) which are connected in parallel fashion may be empowered immediately for more than 2 min in the wake of being charged for 25 s, using supercapacitors comprising of porous carbon, at a current density of  $10 \text{ A g}^{-1}$ . What's more, the porous carbon displays a high reversible charge capacity of  $2120 \text{ mA h g}^{-1}$  in the first cycle (estimated at  $0.1 \text{ A g}^{-1}$ ) or  $1035 \text{ mA h g}^{-1}$  after 300 cycles (estimated at  $1 \text{ A g}^{-1}$ ), when used as an anode for Li-ion batteries [9, 26, 27].

#### 4.1 Preparation of porous carbon for superior energy storage

Devices having energy due to chemical reactions are getting more fame than other energy storage devices due to their considerable potential applications [28]. An instantaneous charging and discharging capability, which leads toward an efficient power density of about  $10 \text{ kW kg}^{-1}$ , can be observed in supercapacitors. The fabrication flowchart for porous carbon is shown in **Figure 7**.

#### 4.2 Surface and physical properties of porous carbon for superior energy storage

On the other hand, in spite of having longer charging time, a high energy density of about  $100\text{--}200 \text{ W h kg}^{-1}$  can be referred in lithium-ion batteries (LIBs). There are two fundamental processes by which the energy can be stored in supercapacitors, which are as follows: (i) pseudocapacitive electrodes store ions based on quick faradaic reactions at the electrode-electrolyte interface, and (ii) electrical double-layer capacitive electrodes store energy by the adsorption and desorption of ions on the large surface area of the porous material [29, 30]. The working of lithium-ion batteries depends upon the transfer of lithium ions in between the cathode and the anode. The mechanism by which the lithium ions are stored or released, in lithium-ion batteries, depends upon the nature of the material of which the electrode is made [31]. High electrical conductivity, tailored porosity, and chemical stability are the main features of carbon materials that make their extensive use in many devices such as commercial supercapacitors and lithium-ion batteries (LIBs) [32]. Scientists reveal that in supercapacitors, mesopores and micropores are the main constituents of porous carbon as they provide ion buffering reservoirs, movement of ions and then storage site for ions, respectively. In lithium-ion batteries, the reversible Li-ion storage capacity is retained to an approximation of  $372 \text{ mA h g}^{-1}$ , for graphite, using graphite anode in lithium-ion batteries which interacts with Li-ions to produce a compound,  $\text{LiC}_6$ , that retains the reversible storage capacity to its mention value. In addition, because of the permeable structure, the use of carbon materials as a

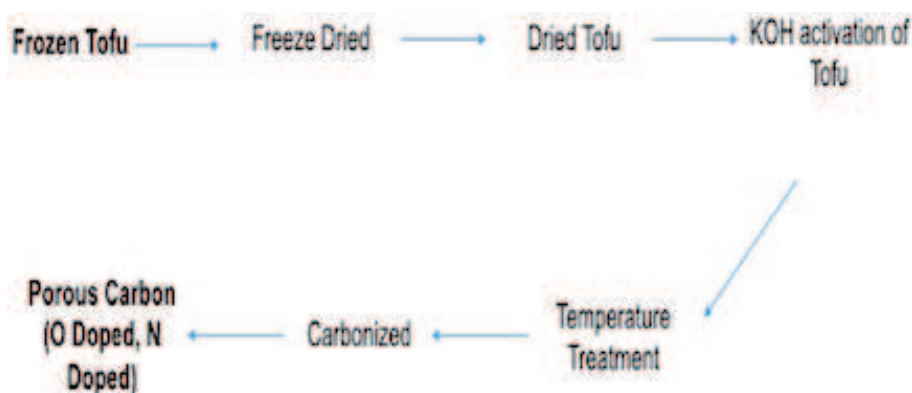


**Figure 7.**

*The fabrication flow chart for porous carbon through one-step carbonization [9].*

framework of electrodes, that is, in lithium-ion batteries and other energy storage devices, is increasing nowadays [33]. It is believed that the supercapacitors cannot fulfill the energy requirements of future electrical devices because of their low energy density (less than  $6 \text{ W h kg}^{-1}$ ). Also, the capacity and rate capability of electrodes in LIBs are below to standards. To approach the above-mentioned requirements, porous carbon having good electrical conductivity and a modified 3-dimensional structure is required [34].

In the recent decades, a number of techniques named activation, self-assembly, and templating have been used for the production of porous carbon materials. But activation exceeds other techniques owing to the fact that it tends to produce a carbon of a large specific surface area of about  $200 \text{ m}^2 \text{ g}^{-1}$  and other useful properties. Activation can also play an important role in the production of novel carbon by doing a proper processing of nanostructured carbon precursors [35]. For instance, graphene platelets can be rebuilt thoroughly to a 3D porous carbon having a specific surface area of approximately  $3100 \text{ m}^2 \text{ g}^{-1}$  and pore size appropriation somewhere in between 0.6 and 5 nm, during the activation of microwave-exfoliated graphite oxide in the presence of KOH. Moreover, in graphite grids, the n-type can be brought up using the atoms like nitrogen which has the ability to donate electrons. The carbon doped with nitrogen finds its applications as anode in lithium-ion batteries because the hybridization between the lone pair electrons of nitrogen with  $\pi$  electrons of carbon can assist lithium lodging [36, 37]. Porous carbon materials derived from biomass are more sustainable than derived from other materials like coal, pitch, polymers, etc. Scientists have indicated that porous carbons for energy stockpiling applications can be acquired from different biomass sources, for example, rice husks, rice straw, algae, what's more, water bamboo. For instance, lithium and other confrere elements experience a one-step pyrolysis-activation synthesis to transform willow catkin into a cross-linked layered porous carbon which is co-doped with two metals, that is, nitrogen (N) and sulfur (S). The carbon thus produced exhibits some outstanding features related to chemical performance like it shows a specific capacitance of  $298 \text{ F g}^{-1}$  at  $0.5 \text{ A g}^{-1}$  in 1 molar solution of  $\text{Na}_2\text{SO}_4$  with the great cycling stability along with the capacitance loss of only 2% when checked after 10,000 cycles at  $5 \text{ A g}^{-1}$ .

Tofu, rich in moisture, proteins, sugars, and follow sums of minerals, is a bounteous asset and has been viewed as a characteristic source of carbon and nitrogen [9, 36, 38]. It is obvious from the above discussion that tofu is a favorable predecessor material in the manufacture of carbon materials used for energy storage devices, but further developments are required for better performance like enhanced capacitance in symmetric supercapacitors and rate capability/cyclic stability in lithium-ion batteries. The features like large surface area, hierarchical (permeable) porous structure, and heteroatomic doping make the use of porous carbon samples (obtained from tofu) suitable for the material used as an anode in Li-ion batteries [9, 35, 38].

## 5. Conclusions

This study presented some novel and modified fabrication techniques for ceramics-graphene hybrids. The improved physical properties may be used to set ceramics-graphene hybrids as a standard for electrical, mechanical, thermal, and energy applications. Further, silica-rGO hybrids may be used as dielectric materials for high temperature applications due to improved dielectric properties. The fabricated nano-assembly is important for a technological point of view, which may be further applied as electrolytes, catalysts, and conductive, electrochemically

active, and dielectric materials for the high-temperature applications. In addition, the porous carbon as a massive source of electrochemical energy for supercapacitors and lithium-ion batteries is also addressed.

### Conflict of interest

The authors have declared no 'conflict of interest'.

IntechOpen

### Author details

Mujtaba Ikram<sup>1\*</sup>, Sana Arbab<sup>1</sup>, Bilal Tariq<sup>1</sup>, Rayha Khan<sup>1</sup>, Husnain Ahmad<sup>1</sup>, Abdullah Khan Durran<sup>1</sup>, Muhammad Ikram<sup>2</sup>, Muhammad Aamir Iqbal<sup>3</sup> and Asghari Maqsood<sup>4</sup>

1 Applied Physics Lab, Institute of Chemical Engineering and Technology (ICET), University of the Punjab (PU), Lahore, Pakistan

2 Department of Physics, Government College University (GCU), Lahore, Pakistan

3 Center for Solid State Physics, University of the Punjab, Lahore, Pakistan

4 Nanoscale Laboratory, Department of Physics, Air University, Islamabad, Pakistan

\*Address all correspondence to: mujtaba.icet@pu.edu.pk

### IntechOpen

© 2020 The Author(s). Licensee IntechOpen. This chapter is distributed under the terms of the Creative Commons Attribution License (<http://creativecommons.org/licenses/by/3.0>), which permits unrestricted use, distribution, and reproduction in any medium, provided the original work is properly cited. 

## References

- [1] Novoselov KS, Fal'Ko VI, Colombo L, Gellert PR, Schwab MG, Kim K. A road map for graphene. *Nature*. 2012;**490**:192-200
- [2] Novoselov KS, Geim AK, Morozov SV, Jiang D, Zhang Y, Dubonos SV, et al. Electric field effect in atomically thin carbon films. *Science*. 2004;**306**:666-669
- [3] Pham VP, Jang H-S, Whang D, Choi J-Y. Direct growth of graphene on rigid and flexible substrates: Progress, applications, and challenges. *Chemical Society Reviews*. 2017;**46**:6276-6300
- [4] Pham PV. The new etching technologies of graphene surfaces. *ACS Omega*. 2018;**3**:8036-8041
- [5] Pham VP, Nguyen MT, Park JW, Kwak SS, Nguyen DHT, Mun MK, et al. Chlorine-trapped CVD bilayer graphene for resistive pressure sensor with high detection limit and high sensitivity. *2D Materials*. 2017;**2**:4
- [6] Pham VP, Jo YW, Oh JS, Kim SM, Jhon MS, Yeom GY. Effect of plasma-nitric acid treatment on the electrical conductivity of flexible transparent conductive films. *Japanese Journal of Applied Physics*. 2013;**52**:7R
- [7] Ikram M, Tao Z, Ye J, Qayyum HA, Sun X, Xu J. Enhanced physical properties of  $\gamma$ -Al<sub>2</sub>O<sub>3</sub>-rGO hybrids prepared by solvothermal and hot-press processing. *RSC Advances*. 2018;**8**: 8329-8337
- [8] Ikram M, Qayyum HA, Ali S, Tan Z, Ahmad M, Xu J. Hydrothermal-hot press processed SiO<sub>2</sub>-rGO hybrid with enhanced physical properties. *Journal of Solid State Chemistry*. 2018;**265C**:364-371
- [9] Sun X, Ye J, Pan F, Xu J, Cheng T, Wang X, et al. Hierarchical porous carbon obtained from frozen tofu for efficient energy storage. *New Journal of Chemistry*. 2018;**42**:12421-12428
- [10] Balazs AC, Emrick T, Russell TP. Nanoparticle polymer composites: Where two small worlds meet. *Science*. 2006;**314**:1107-1110
- [11] Yang X, Zhang X, Ma Y, Huang Y, Wang Y, Chen Y. Superparamagnetic graphene oxide-Fe<sub>3</sub>O<sub>4</sub> nanoparticles hybrid for controlled targeted drug carriers. *Journal of Materials Chemistry*. 2009;**19**:2710-2714
- [12] Stankovich S, Dikin DA, Dommett GHB, Kohlhaas KM, Zimney EJ, Stach EA, et al. Graphene-based composite materials. *Nature*. 2006;**442**:282-286
- [13] Zhang Z, Pinnavaia TJ. Mesostructured  $\gamma$ -Al<sub>2</sub>O<sub>3</sub> with a Lathlike framework morphology. *Journal of the American Chemical Society*. 2002;**124**:12294-12301
- [14] Ahmad I, Cao H, Chen H, Zhao H, Kennedy A, Zhu YQ. Carbon nanotube toughened aluminium oxide nanocomposite. *Journal of the European Ceramic Society*. 2010;**30**:865-873
- [15] Jagminas A, Kaciulis S, Klimas V, Reza A, Mickevicius S, Soltani P. Fabrication of graphene-alumina heterostructured films with nanotube morphology. *Journal of Physical Chemistry C*. 2016;**120**:9490-9497
- [16] Benavente R, Pruna A, Borrell A, Salvador MD, Pullini D, Penaranda-Foix F, et al. Fast route to obtain Al<sub>2</sub>O<sub>3</sub>-based nanocomposites employing graphene oxide: Synthesis and sintering. *Materials Research Bulletin*. 2015;**64**:245-251
- [17] Liu Y, Ma D, Han X, Bao X, Frandsen W, Wang D, et al. Hydrothermal synthesis of microscale

boehmite and gamma nanoleaves alumina. *Materials Letters*. 2008;**62**:1297-1301

[18] Chen YF, Lee CY, Yeng MY, Chiu HT. The effect of calcination temperature on the crystallinity of TiO<sub>2</sub> nanopowders. *Journal of Crystal Growth*. 2003;**247**:363-370

[19] Zhang Y, Li D, Tan X, Zhang B, Ruan X, Liu H, et al. High quality graphene sheets from graphene oxide by hot-pressing. *Carbon*. 2013;**54**:143-148

[20] Liu H, Choy KL, Roe M. Enhanced conductivity of reduced graphene oxide decorated with aluminium oxide nanoparticles by oxygen annealing. *Nanoscale*. 2013;**5**:5725-5731

[21] Wang SX, Zou KX, Qian YX, Deng YF, Zhang L, Chen G.H. et al. Insight to the synergistic effect of N-doping level and pore structure on improving the electrochemical performance of sulfur/N-doped porous carbon cathode for Li-S batteries. *Carbon* 2019;**144**:745-755

[22] Nan CW, Shen Y, Ma J. Physical properties of composites near percolation. *Annual Review of Materials Research*. 2010;**40**:131-151

[23] Kim JY, Lee WH, Suk JW, Potts JR, Chou H, Kholmanov IN, et al. Chlorination of reduced graphene oxide enhances the dielectric constant of reduced graphene oxide/polymer composites. *Advanced Materials*. 2013;**25**:2308-2313

[24] Zaretsky EB. High temperature impact response of 998 alumina. *Journal of Applied Physics*. 2013;**114**:183518

[25] Yoo E, Kim J, Hosono E, Zhou H-s, Kudo T, Honma I. Large Reversible Li Storage of Graphene Nanosheet Families for Use in Rechargeable Lithium Ion Batteries. *Nano Letters*. 2008;**8**:2277-2282

[26] Wang L, Zhang G, Zhang X, Shi H, Zeng W, Zhang H, et al. Porous ultrathin carbon nanobubbles formed carbon nanofiber webs for high-performance flexible supercapacitors. *Journal of Materials Chemistry A*. 2017;**5**:14801-14810

[27] Kang K, Meng YS, Bréger J, Grey CP, Ceder G. Electrodes with high power and high capacity for rechargeable lithium batteries. *Science*. 2006;**311**:977-980

[28] Staaf L, Lundgren P, Enoksson P. Present and future supercapacitor carbon electrode materials for improved energy storage used in intelligent wireless sensor systems. *Nano Energy*. 2014;**9**:128-141

[29] Wang B, Zhang W, Wang L, Wei J, Bai X, Liu J, et al. Three dimensional carbon-bubble foams with hierarchical pores for ultra-long cycling life supercapacitors. *Nanotechnology*. 2018;**29**:275706

[30] Shopsowitz KE, Hamad WY, MacLachlan MJ. Chiral nematic mesoporous carbon derived from nanocrystalline cellulose. *Angewandte Chemie, International Edition*. 2011;**50**:10991-10995

[31] Zhu Y, Murali S, Stoller MD, Ganesh K, Cai W, Ferreira PJ, et al. Carbon-based supercapacitors produced by activation of graphene. *Science*. 2011;**332**:1537-1541

[32] Sankar S, Lee H, Jung H, Kim A, Ahmed ATA, Inamdar AI, et al. Ultrathin graphene nanosheets derived from rice husks for sustainable supercapacitor electrodes. *New Journal of Chemistry*. 2017;**41**:13792-13797

[33] Sevilla M, Fuertes AB. Hierarchical microporous/mesoporous carbon nanosheets for high-performance supercapacitors. *ACS Nano*. 2014;**8**:5069-5078

[34] Sing KS. Reporting physisorption data for gas/solid systems with special reference to the determination of surface area and porosity. *Pure and Applied Chemistry*. 1985;**57**:603-619

[35] Zhou Q, Chang J, Jiang Y, Wei T, Sheng L, Fan Z. Fast charge rate supercapacitors based on nitrogen-doped aligned carbon nanosheet networks. *Electrochimica Acta*. 2017;**251**:91-98

[36] Yang G, Niu J, Shao R, Liang J, Dou M, Li Z, et al. A facile molecularly engineered copper (II) phthalocyanine as hole transport material for planar perovskite solar cells with enhanced performance and stability. *Nano Energy*. 2017;**36**:322-330

[37] Fang Y, Lv Y, Che R, Wu H, Zhang X, Gu D, et al. Two-dimensional mesoporous carbon nanosheets and their derived graphene nanosheets: Synthesis and efficient lithium ion storage. *Journal of the American Chemical Society*. 2013;**135**:1524-1530

[38] Hou J, Cao C, Idrees F, Ma X. Hierarchical porous nitrogen-doped carbon nanosheets derived from silk for ultrahigh-capacity battery anodes and supercapacitors. *ACS Nano*. 2015;**9**:2556-2564